Absolute optical chiral analysis using cavity-enhanced polarimetry

Lykourgos Bougas[1]*, Joseph Byron[2], Dmitry Budker[1,3,4], and Jonathan Williams[2,5]

Chiral analysis is central for scientific advancement in the fields of chemistry, biology, and medicine. It is also indispensable in the development and quality control of chiral compounds in the chemical and pharmaceutical industries. Current methods for chiral analysis, namely optical polarimetry, mass spectrometry and nuclear magnetic resonance, are either insensitive, have low time resolution, or require preparation steps, and so are unsuited for monitoring chiral dynamics within complex environments: the current need of both research and industry. Here we present the concept of absolute optical chiral analysis, as enabled by cavity-enhanced polarimetry, which allows for accurate unambiguous enantiomeric characterization and enantiomeric-excess determination of chiral compounds within complex mixtures at trace levels, without the need for calibration, even in the gas phase. The utility of this approach is demonstrated by post chromatographic analysis of complex gaseous mixtures, the rapid quality control of perfume mixtures containing chiral volatile compounds, and the online in-situ observation of chiral volatile emissions from a plant under stress. Our approach and technology offer a step change in chiral compound determination, enabling online quality control of complex chemical mixtures, identification of counterfeit goods, detection of pests on plants, and assessment of chiral emission processes from climate relevant ecosystems.

Main

Chiral analysis — enantiomeric characterization and enantiomeric excess (e.e.) determination — is a challenging task as the chemical and physical properties of enantiomers are identical so enantiomers can only be distinguished through their interaction with another chiral object[1]. For this reason, analytical techniques such as optical polarimetry, mass spectrometry (MS) and nuclear magnetic resonance (NMR), rely on the chirality of light or of a molecular environment (as in the case of chiral chromatography)[1–3]. These techniques, however, require extensive calibrations for accurate analysis and typically fail to reliably detect chiral compounds at trace levels within complex mixtures. Modern chirality sensitive optical techniques such as photoionization[4–6], femtosecond[7], microwave[8], and superchiral-light-based[9,10] spectroscopies, offer specific advantages, including sensitivities sufficient for gas-phase sensing or the detection of protein monolayers. Yet such techniques cannot currently operate within complex environments such as chiral sensing in ambient air. Most crucially, the overall inability of all aforementioned techniques to allow for accurate real-time measurements without the need for calibration prevents in-situ real-time study of important chemical, biological, and medical dynamical processes, such as the response of biological organisms to sickness[11,12] or stress[13].

Molecular optical activity measurements remain the best option to address these limitations[3]. Optical rotary dispersion (ORD) and circular dichroism (CD), in particular, remain the most widely used techniques for measuring chirality[2]. However, molecular chiroptical signals are intrinsically weak (~10^{-5}

[1] Institut für Physik, Johannes Gutenberg-Universität Mainz, Mainz, Germany

[2] Max-Planck-Institut für Chemie, Mainz, Germany

[3] Helmholtz Institute Mainz, GSI Helmholtzzentrum für Schwerionenforschung, Darmstadt, Germany

[4] Department of Physics, University of California, Berkeley, CA, USA

[5] Climate and Atmosphere Research Center, The Cyprus Institute, Nicosia, Cyprus.

* Correspondence should be addressed to: bougas.lykourgos@gmail.com

– 10^{-3} rad) and often masked by dominant backgrounds. As a result, the application of chiral analysis by ORD and CD measurements has remained limited to the detection of high-concentration samples, in particular liquids. Recently, a polarimetric technique for enhanced ORD and CD measurements was developed, dubbed cavity-enhanced chiral polarimetry (CCP)[14–18]. CCP employs a ring (four-mirror) optical cavity in a bowtie configuration, where the light always passes through the chiral sample from the same direction, to enhance the chiroptical signals (ORD, CD) by the large number of cavity passes (optimally $>10^4$); **Fig.1**. Crucially, the placement of an intracavity Faraday rotator, in relation to the symmetry of natural optical activity and the available counter-propagating modes of propagation within the cavity, enables crucial signal-reversal operations that allow for absolute polarimetric measurements not requiring sample removal for a null-sample measurement or instrument calibration[16–18]. To date, however, all CCP experiments have reached only poor chiral detection limits (~μrad/pass) within relatively long integration times (~min)[16–19], conditions that have hindered the extension of CCP to real-time chiral analysis.

Absolute optical chiral analysis can allow for: (1) absolute enantiomeric identification and direct, accurate, determination of the intrinsic specific optical rotation of a chiral compound without the need for calibration; (2) the discrimination of chiral from achiral compounds within complex mixtures and direct estimation of their relevant concentrations; and (3) absolute enantiomeric excess determination. The enhanced signal-detection capability offered by CCP allows one to perform these detection capabilities in the gas phase and under a wide range of conditions, such as direct air sampling and/or headspace analysis. In addition, CCP being a cavity-enhanced spectroscopy allows for the sensitive measurement of the average refractive index of the intracavity medium (as cavity resonances depend on the refractive index of the medium), which becomes critical in accurately quantifying unknown compounds and/or distinguishing chiral from achiral compounds. Here we present optical-based absolute chiral analysis in the gas phase, as this is enabled through CCP and a measurement scheme based on frequency metrology[20–22]. Using our approach, we demonstrate: (1) the absolute chromatographic analysis of complex mixtures in the gas-phase without the need for calibration; (2) the real-time, rapid, quality control of complex mixtures containing both chiral and achiral compounds as a means to identify purity or authenticity, and (3) the in-situ monitoring of chiral emissions from a biological organism, a plant, under abiotic, i.e., mechanical, stress.

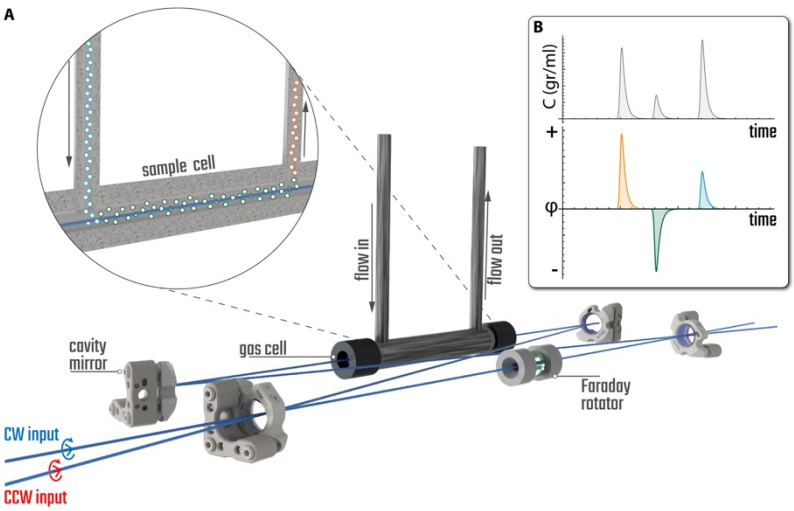

Figure 1| **Chiral analysis using cavity-enhanced chiral polarimetry (CCP). A.** Schematic of CCP showing the four mirrors of the optical cavity arranged in a bowtie configuration, the optical beam paths of the allowed counter-propagating laser beams (CW and CCW), the Faraday rotator, and the gas cell. **B.** The absolute measurement character of CCP allows for direct enantiomer characterization and accurate enantiomeric excess determination without the need for calibration via the use of chromatography or a total-sample analysis modality.

Gas phase chiral analysis using GC/CCP

State-of-the-art chiral analysis, especially in the gas phase, is largely performed using MS-based techniques. MS-based chiral analysis can be realized in combination with different methodic approaches, such as chiral chromatography or chemical reactions with chiral reference molecules[23]. In all instances, however, extensive calibrations are necessary for accurate quantification of the results and, hence, accurate e.e. determination (i.e., non-absolute measurement). Furthermore, specifically in the case of employing chromatography, the elution order of enantiomers depends both on the chosen column and separation method and can be different for different compounds, which complicates enantiomeric identification.

We demonstrate here how CCP-based absolute chiral analysis overcomes these limitations, specifically by focusing on gaseous samples. In **Fig.2A** we present the specific optical rotatory power $[\alpha]_{\lambda}^{T}$ for several gaseous chiral volatile organic compounds (VOC), particularly monoterpenes (additional data are taken from Refs.[17,19,24,25]). In polarimetric-based chiral analysis, the specific optical rotation (SOR) of a substance at a given wavelength can be used to convert the acquired polarimetric signal to concentration. Furthermore, our approach allows us to detect, and distinguish between, the average refractive index and the chirality parameter of a chiral substance (or even a mixture). As such, when analyzing complex mixtures that may contain both chiral and achiral compounds, we are able to distinguish these without influencing the quantification of the attainable results. We demonstrate these advantages by combining gas-chromatography (GC) with CCP-based chiral detection, i.e., GC/CCP. In particular, in **Fig.2B** we show the optical rotation (OR-) chromatogram, i.e., φ vs. retention time, of a mixture containing several monoterpenes in enantiopure or racemic form, and in **Fig.2C** the OR-chromatogram for the case of racemic limonene. In both cases we can identify the enantiomers of the eluted compounds through the sign of their chiroptical signal, while the refractometric measurements directly reflect their relative concentrations within the prepared mixtures (this feature becomes particularly crucial in the analysis of a compound with unknown specific rotation). Here, gas-phase detection takes place under ambient conditions with the mobile phase being directly expanded into the instrument's intracavity gas cell (**Fig.1**) (similarly to the operating conditions of GC-olfactometry[26]). For this reason, in conjunction with an incomplete separation, in the case of racemic limonene (**Fig.2C**) we observe a single refractometric feature; yet the polarimetric signal allows us to accurately identify the racemic character of the mixture by resolving both enantiomers having equal densities. Crucially, the absolute character of CCP-based detection allows us to accurately and directly infer the elution order of the two enantiomers (in **Fig.S1** we also present the OR-chromatograms for the enantiopure cases). Furthermore, in **Fig.2D** we show the OR-chromatogram for the case of enantiopure (R)-(-)-2-butanol. The refractometric signal (δη; **Fig.2D,** upper panel) reflects both the solvent and the chiral compound. This allows us to quantify the relative concentration of the target compound within the solution, while the OR signal depends solely on the specific OR of (R)-(-)-2-butanol and its concentration. This is in contrast to traditional MS-based detection schemes, where coeluting chiral/achiral compounds are indistinguishable hindering, thus, accurate characterization and quantification.

An additional advantage of CCP-based chiral analysis is the ability to perform a total sample analysis via, for instance, dynamic air or headspace sampling (i.e., without using pre-separation techniques such as GC). In **Figs.2B-D** we compare the GC/CCP results with their respective total sample measurements. Here, these measurements are realized under ambient conditions using dynamic open-air sampling of the chiral vapors of the mixtures prepared for the GC analysis, i.e., without the need for additional sample preparation. In this case, the overall OR signal is equal to the sum of the individual specific rotations from each compound within the mixture times their respective concentrations, which in turn

relate to their partial pressures ($\varphi_{\text{tot.}} = \sum_i c_i \cdot [\alpha]_i$, where $\varphi_{\text{tot.}}$is the measured total OR signal, with c_i and $[\alpha]_i$ the amount-of-substance faction and SOR, respectively, of each component in the mixture). For the analysis, we normalize the recorded total sample OR signals over their corresponding concentration (as obtained from the refractometric signals[27]). This yields an effective specific rotation for each mixture (in the case of a single compound, such a measurement yields its SOR, $[\alpha]_\lambda^T$; **Fig.2A-C**). We demonstrate that such a total sample analysis is in accord with the GC/CCP analysis for all examined cases. Most importantly, for the case of single-chiral-compound analysis (either within a solution or neat), we find that, as in the case of **Fig.2C** where we present the signals for enantiopure (+)/(-)-limonene, this approach allows for direct, rapid, e.e. determination. Considering our current polarimetric sensitivity and the attainable OR signals for the case of, for instance, limonene (**Fig.2A,C**), we can determine gas-phase e.e. at levels better than <1% even under high-noise conditions (dynamic ambient air sampling), within ~1s of integration time (for the total-sample analysis we present in, e.g., **Fig.2C**, the statistical uncertainties originate from the dynamic air sampling).

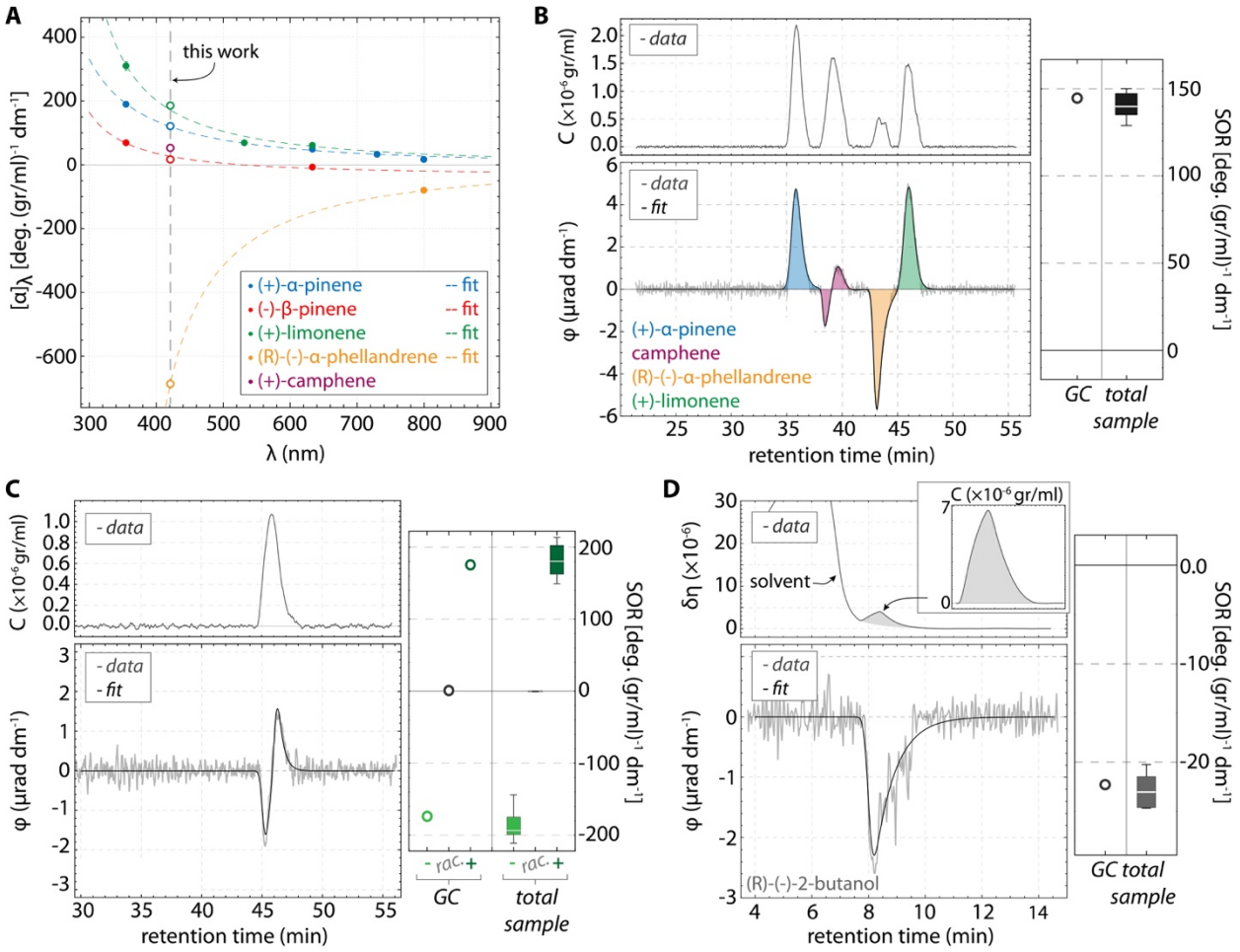

Figure 2 | **CCP-based absolute gas-phase chiral analysis using gas chromatography (GC) and direct total-sample measurement. A.** Variation of the specific optical rotation (SOR) of different monoterpenes as a function of wavelength, showing our measurements at 421nm. **B-D.** CCP-based chiral analysis using GC of a mixture of several monoterpenes (**B**), of racemic limonene (**C**) and of enantiopure (R)-(-)-2-butanol (**D**). The OR-chromatograms (φ vs. retention time) allow for direct enantiomeric characterization and quantitative enantiomeric excess determination. The concentration of each analyte is directly extracted through the refractometric measurements (upper panels **B-D**) but can be also extracted from the rotation signal (through the SOR). The refractometric measurements also allow us to distinguish achiral and chiral compounds, even when these are coeluting (**D**). We compare the results obtained from GC/CCP analysis with chirality measurements of the vapours of each mixture, i.e., a total-sample analysis, under conditions of direct air sampling. Box-and-whisker plot analysis of total-sample chirality measurements (the white line represents the mean, the box height represents 1σ confidence intervals, while the bars represent the maximum and minimum acquired data points). Each box results from the statistical analysis of at least seven measurements performed under ambient conditions using direct air sampling (~20s of sampling). In all cases, we find our total-sample analysis to be in accord with the GC/CCP measurements.

Real-time quality control via optical chiral analysis

The ability to perform a total-sample analysis and measure the overall chiroptical signal of a complex mixture in an absolute manner, opens up the possibility for accurate quality control analysis in real time. Such a possibility is essential, for instance, in rapidly identifying purity and even authenticity. In the simplest case, a mixture produced using racemates or through chemical synthesis that does not incorporate any enantioselective procedure[28] (e.g., chiral reactants and catalysts[29] or magnetic structures[30]), will be racemic and, hence, its overall OR signal will be zero. In contrast, if such a mixture is produced using natural material sources or enantioselective synthesis, then, in general, it should be chiral, yielding a non-zero OR signal whose sign reflects the chirality of the dominant enantiomers (e.g., **Fig. 2C-D**). Furthermore, the ability to simultaneously measure the overall concentration of all volatile (achiral/chiral) components within a complex mixture allows us, in turn, to accurately determine the concentration of the chiral components within it.

An exemplar model of a complex chemical mixture containing both achiral and chiral VOCs is perfume, which typically consists of both natural (originating from essential oils) and synthetic organic compounds. A perfume's quality relies on its fragrance profile, and detailed determination of its composition, i.e., perfume formulation, requires analytical techniques such as GC/MS. This becomes

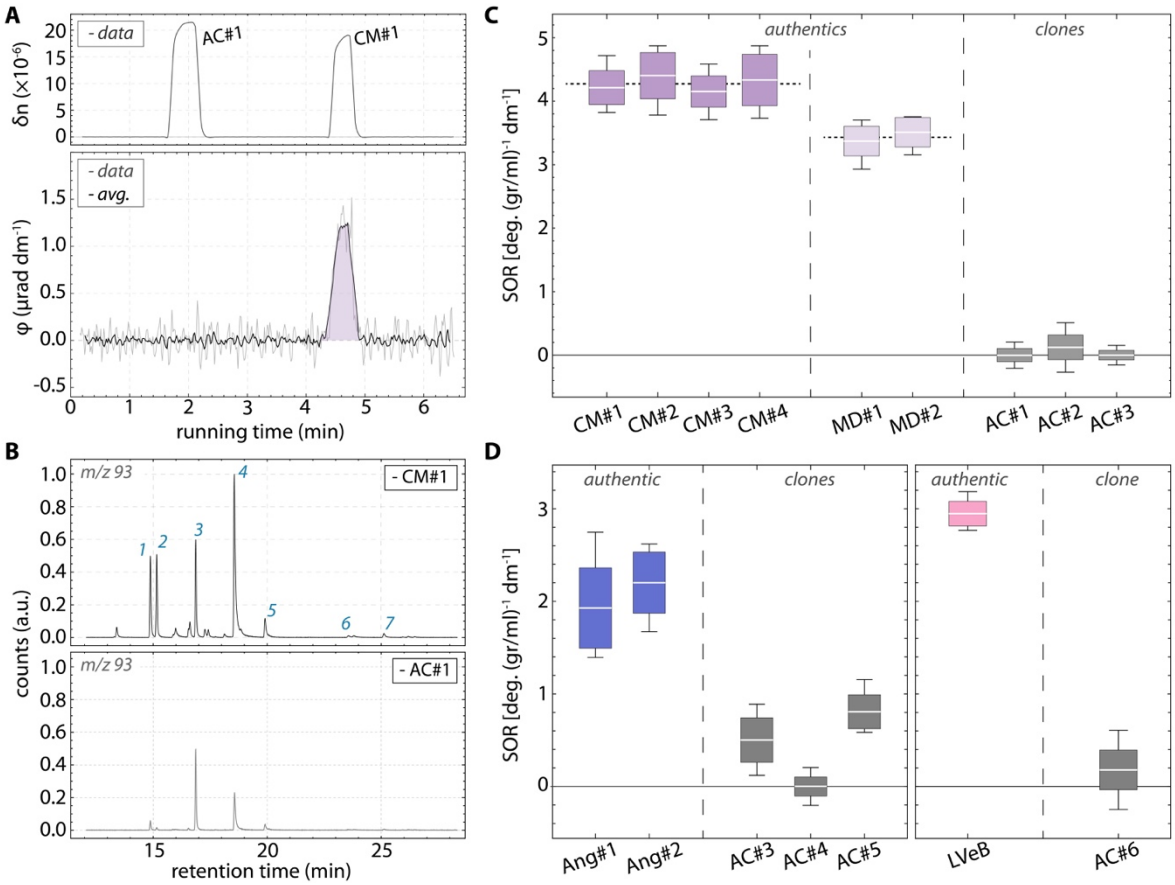

Figure 3 | **Perfume quality control using CCP-based absolute chiral analysis**. **A.** Real-time CCP measurements of an authentic perfume ('*Coco Mademoiselle*' by Chanel; CM) vs one of its low-cost fragrance clones (AC#1), under conditions of direct ambient-air sampling. Time separation between measurement points is 0.5s (i.e., equal to the integration time for each measurement). **B.** GC/MS chromatograms of 'CM' (CM#1) and of AC#1 revealing the following dominant chiral volatile compounds: ***1*** (-)-α-pinene; ***2*** (+)-α-pinene; ***3*** (-)-β-pinene; ***4*** (+)-limonene; ***5*** γ-terpinene; ***6*** (-)-linalool followed by (+) linalool; and ***7*** linalyl acetate. **C-D.** Box-and-whisker plot analysis comparison of chiroptical measurements for different authentic perfumes (CM, MD, Ang, LVeB; see Methods for details) vs their respective low-cost alternatives. The white lines represent the mean, the box heights represent 1σ confidence intervals, while the bars represent the maximum and minimum acquired data points. Each box results from the statistical analysis of at least seven measurements performed under ambient conditions using dynamic air sampling (~20s of sampling). Overall, absolute chiral analysis allows for accurate, quantitative, quality control of authentic perfumes while enabling the rapid identification of a perfume imitation.

particularly complex in analytical quality control, considering that perfumes consist of several hundred or even thousands of different compounds. Notwithstanding, chemical fingerprinting can also be employed for quality control, which can enable rapid, real-time, quality analysis becoming, in turn, vital in identifying, for instance, counterfeit perfumes.

We demonstrate here how absolute optical chiral analysis can be used for the (rapid) quality control of perfumes directly in the gas phase without any sample preparation (e.g., possible via dynamic air sampling through nebulizing from the original bottle). By measuring the overall chiroptical signal of a perfume we obtain a distinct dynamic chiral signature rather than a multi-component spectrum as in the case of MS-based schemes, i.e., chiral fingerprinting. For our demonstrations we use four (4) authentic perfumes (eau de parfum): '*Coco Mademoiselle*' ('CM') by Chanel, '*Miss Dior*' ('MD') by Dior, '*Angel*' by Thierry Mugler, and '*La vie est belle*' ('LVeB') by Lancôme. As model counterfeit/adulterated samples we use their, commercially available, low-cost fragrance clones (see Methods for an extensive list). Low-cost clones also contain compounds originating from natural or enantiopure sources and are, thus, particularly suitable for a quantitative quality comparison (a fully synthetic perfume, where any chiral molecule would be present in racemic form, will yield a null chiroptical signal). In **Fig.3A** we show a real-time comparison between the observed ambient signal for an authentic perfume ('CM'), and one of its low-cost clones, in which the authentic perfume yields a positive chiral signal whereas the clone a null signal. GC/MS analysis reveals that the observed differences in the chiral OR signals cannot be attributed to a single component but to an overall difference in compositions [e.g., (-)-β-pinene is the dominant component in the low-cost alternative vs. (+)-limonene in the authentic perfume; **Fig.3B**]. GC/MS analysis allow us to corroborate the positive chiral character of the authentic perfume, attributed to (+)-limonene, which is the dominant monoterpene in most citrus-based essential oils[31]. The observed null signal for the fragrance clone (AC#1, **Fig.3A**), however, indicates that any chiral substances present within its matrix (**Fig.3B**) are at much lower concentrations than in the authentic perfume, and in this case at concentrations lower than our current detection limits. Additionally, the refractometric signals – largely dominated by the alcohols that have the highest concentration (70%-80%) within the perfumes – allow us to record distinct differences between the matrices of the two perfumes assisting identification **(Fig.3A)**. Using both refractometric and chirality measurements, we present in **Fig.3C-D** an overall comparison between the chiral signatures of several authentic perfumes with their respective low-cost fragrance clones. We also perform measurements on samples from different (purchased) bottles for each of the authentic perfumes to establish the validity of our approach towards quality control. We observe similar chiroptical signals for the same perfume from different packages. Overall, we demonstrate that we can accurately, and in a quantitative manner, distinguish high-quality perfumes from each other and from their low-cost clones using their chiroptical signatures, as these originate from differences in their composition and even possible adulteration. Particularly for the case of the authentic 'CM' and 'MD', the similarities between their monoterpene chromatograms (**Fig. S2**) suggest that considerable analysis using, for instance, chiral-GC/MS is required to accurately distinguish them. In contrast, absolute optical chiral analysis enables us to distinguish between them directly in a rapid single measurement using their distinct chiral signatures.

Online in-situ chiral analysis of VOC emissions from biological organisms

Real-time absolute chiral analysis in the gas phase opens up the possibility for observing in situ the emissions of chiral VOCs from biological organisms such as plants. An estimated of ~760Tg (C) of biogenic VOCs (BVOCs) enter the Earth's atmosphere every year primarily from terrestrial vegetation[32] (contributing also to the production of secondary organic aerosols that affect the Earth's radiative budget[33]). BVOC emissions are the result of the biological functions of plants, i.e., their metabolism and response mechanisms, and serve as the plant's main communication and interaction channel with the surrounding environment[13]. Specifically, plants release BVOCs into the surrounding air in response to both abiotic (e.g., light or soil conditions) and biotic (e.g., herbivores or pests) stress factors[34,35]. Monoterpenes are among the most abundant BVOC species observed in the atmosphere (~11%)[32], many of which are chiral and naturally exist as enantiomeric pairs in the atmosphere at mixing ratios of $\lesssim$ppbv[36,37]. Yet, their chiral nature is largely ignored in air-chemistry studies and related models[32], as their enantiomers are not quantified separately and are modelled as having similar source characteristics, based on their identical physical properties (boiling point, exact mass) and observed reaction rates with oxidants. Similarly, studies of BVOC emissions from individual plants largely ignore their chiral nature, despite the fact that chiral chemodiversity within a plant's VOC emission profile has a critical role both in (mutually benefiting) plant–insect[38–40] and plant–plant[41–43] interactions.

Recent air-chemistry studies have revealed puzzling effects that stress the need to investigate the role of chirality in BVOC emissions. These unexpected effects are: (i) regiospecific behaviour in the enantiomers of BVOCs, such as α-pinene[44]; (ii) diurnal enantiospecific enhancements in BVOC emissions in boreal forests[45,46]; (iii) enantiospecific compositional changes of BVOCs over the Amazon forest as a function of altitude, time and season[37]; and, (iv) compartment enantiospecific emissions identified in coniferous trees[47–49]. These findings reveal gaps in our understanding of how emissions are controlled and modelled[32,50], particularly considering that processes in the atmosphere such as photo-oxidation are not expected to be enantioselective, whereas microbial degradation[51] and plant metabolism[13] are. Air-chemistry studies are, almost in their entirety, realized using MS-based analysis, which requires chiral gas chromatography (GC) to quantify enantiomers separately. Such studies, therefore, typically require on-site sampling that leads to poor time resolutions (samples are typically collected every ~2-3hrs)[37,46,49] and often difficult-to-predict uncertainties during offline analysis[52,53].

Here, we measure the chirality of the volatile emissions of a plant under mechanical wounding, in situ. The principal motivation for such a measurement is the initiation of a thorough investigation on mechanical damage as a stress mechanism responsible for the observed chiral composition changes of VOCs over different ecosystems, such as boreal forests[54,55] and the Amazon rainforest[37]. Here, we use a coniferous plant, a *Pinus heldreichii* (**Fig. 4A**), and record the chiral dynamics of its branch emissions following mechanical wounding, i.e., the complete cut of one of the branches of the plant. For comparison, but also as validation of our approach with state-of-the-art techniques used in similar studies, we employ together with our online CCP-based measurements an offline chiral-GC/MS-based analysis.

We first measure the plant emissions for several hours prior to wounding to establish a baseline for their overall concentration and chiral OR signal with our online CCP measurement. Using the offline GC/MS analysis we are additionally able to establish the compositional character of the branch emissions (sampling times for the online and offline measurements are 15 and 10min, respectively). In the resting state, the dominant chiral VOCs in the plant emissions are monoterpenes that primarily originate from *de novo* synthesis and evaporation from storage structures[56,57]. The CCP-based measurements reveal an overall concentration of the emitted monoterpenes at the ~1ppmV levels and

a negative chiral OR signal (**Figs.4B-D**). The offline GC/MS analysis allows us to specifically identify (±)-α-pinene, (±)-camphene, (-)-β-pinene and (±)-limonene, as the principal monoterpene VOCs in the plant emissions, and to corroborate the concentration measurement of the plant emissions with our CCP measurements (**Figs.4E**). Additionally, from the GC spectra we observe that (-)-limonene dominates the overall emission profile, confirming thus the overall recorded negative OR signal, while we see that the (+)-α-pinene isomer prevails over its (-)-isomer.

Following mechanical wounding we observe an abrupt ~10-fold increase in the concentration of the plant emissions that drop with a characteristic time of ~4h to stabilize at densities approaching their pre-wounding values, in accordance with similar observations in the literature[58]. Such a dynamical behavior is established by both online and offline measurements (**Fig.4C**). The chiroptical OR signal (**Fig.4D**), however, becomes more negative to reach a maximal negative value within ~6h from the

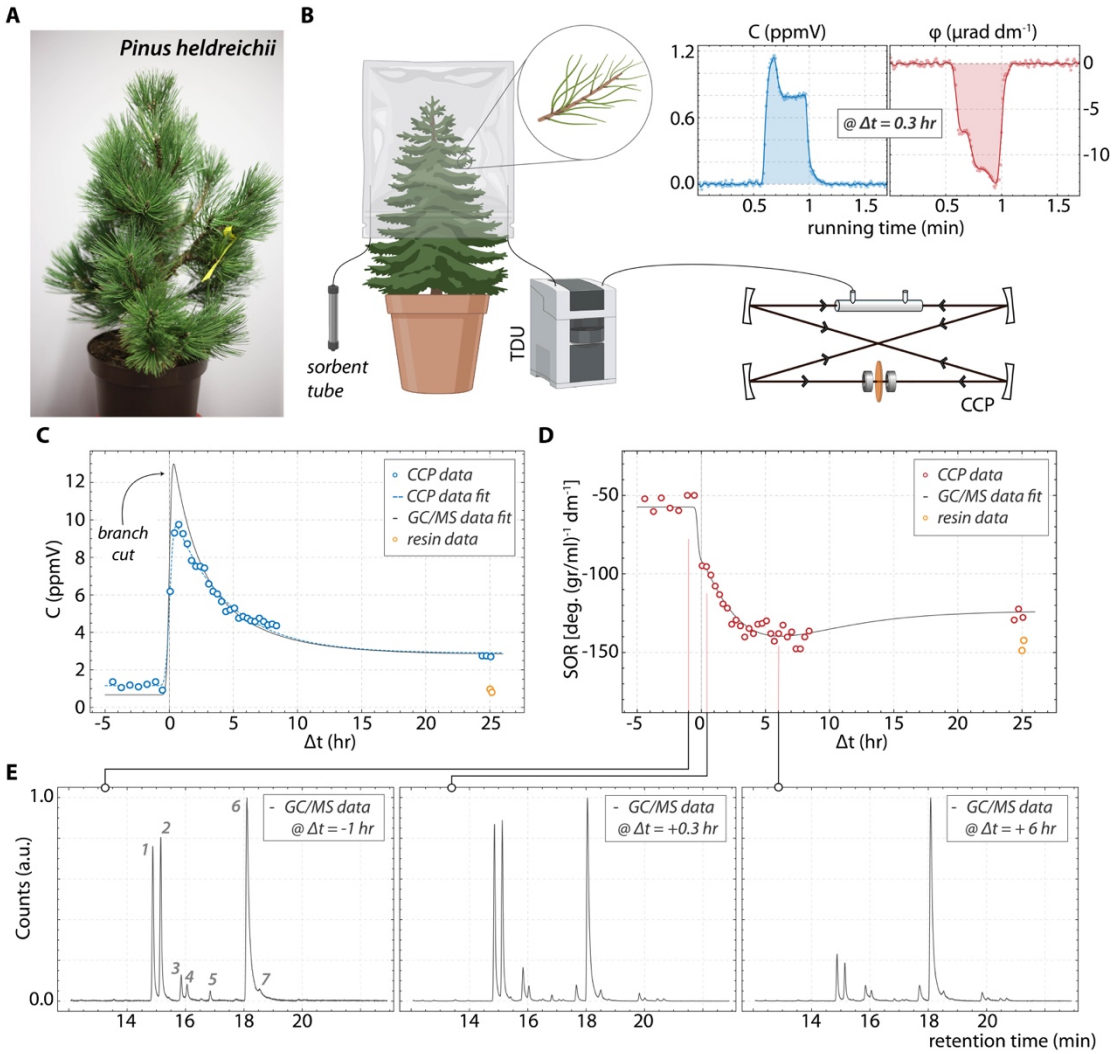

Figure 4 | **Online in-situ chirality measurements of the emissions of a coniferous plant during mechanical wounding. A.** Photo of the coniferous plant used in the measurements, *Pinus heldreichii*. **B.** Schematic of the setup required to sample and measure the chirality of the VOC emissions from the branches of the plant (pre- and post-wounding) using CCP (TDU: thermal desorption unit). Sorbent tubes are required for the offline chiral-GC/MS analysis. Insets show post-wounding CCP measurements revealing the presence of different compounds in the emissions and an overall negative optical rotation (OR) signal. **C - D.** Concentration (as obtained through refractometric measurements and corroborated via GC/MS analysis) and OR signals (normalized over concentration). Yellow points correspond to concentration and chirality measurements from the secreted resin that covers the wounding site. **E.** GC/MS chromatograms for different times pre- and post- wounding. The spectra are normalized over their respective signal value for (-)-limonene (peak 6), to visually aid the comparison between the relative signal changes among all eluted compounds. Labeled peaks: ***1*** (-)-α-pinene; ***2*** (+)-α-pinene; ***3*** (-)-camphene; ***4*** (+)-camphene; ***5*** (-)-β-pinene; ***6*** (-)-limonene; ***7*** (+)-limonene.

wounding [approaching the specific rotation value for enantiopure (-)-limonene, see **Fig.2A**], while stabilizing long-term to an OR signal value that is more negative than its initial (prior to wounding) resting one. The observation of such a distinct difference between the dynamics in the chiroptical OR signal and those of the overall VOC concentration signal directly reveal the presence of chirally specific differences in the dynamic behavior of different monoterpene isomers and their respective enantiomers. Specifically, our refractometric measurements (**Figs.4B**), corroborated by the GC/MS analysis (**Fig.4E and Fig.S7**), allow us to identify that the observed chiral dynamics, towards more negative values, are the result of the dominance of (-)-limonene in the overall emission profile and of a relative increase in the (-)-α-pinene enantiomer over its (+)-enantiomer [which, in turn, is in accord with observations from other studies and in line with the results obtained from the relevant Amazon measurements[37]]. To provide further insight into the observed chiroptical signals, we independently record also the chiral OR signal from the resin secreted by plant's storage ducts that eventually hardens to seal the wound site (**Fig. S8**). The long-term recorded OR signal value of the plant emissions is close to the OR signal value obtained independently from the resin (**Fig. 4C-D**), indicating that chiral VOC composition of the resin dominates the overall emission profile of the plant in the long-term, following mechanical wounding.

Discussion

Optical-based technologies hold the potential for surpassing critical limitations in current state-of-the-art techniques used for chiral analysis, such as MS and NMR. We demonstrate how continuous-wave cavity-enhanced optical polarimetry, specifically CCP through the implementation of a frequency-metrology measurement scheme, enables real-time chiral analysis of complex chemical mixtures in an absolute manner, i.e., without the need for calibration, at trace quantities (e.g., gas phase).

Specifically, we first demonstrate the CCP-based absolute chiral analysis of gaseous mixtures using GC. Our current instrument sensitivity is ~3.4×10^{-7}rad/√Hz (~20μdeg within 0.5s of integration time) and is ultimately limited by photon shot noise at the 1.3×10^{-9}rad/√Hz level. Considering the typical values for the SOR of monoterpenes [~100deg. (gr/ml)$^{-1}$dm^{-1}; **Fig.2A**], such limits correspond, respectively, to gas sensitivities of ~35ppmV√Hz and ~131ppbV√Hz. Instrument and technique improvements, however, which may include the use of a higher-finesse optical cavity, higher-quality intracavity optics and alternative detection schemes, can lead to chiroptical sensitivities of ~10^{-13}rad/√Hz[20,21], which correspond to concentration sensitivities of <10pptV√Hz. Such sensitivities match those attainable with current state-of-the-art MS-based detection methodologies.

Second, we demonstrate rapid analysis of complex chemical mixtures containing both chiral and achiral compounds using their distinct gas-phase chiral signatures. As our target system, we select perfume, complex mixtures that contain both achiral and chiral compounds. Accurate, quantitative, component analysis of perfumes is typically performed using GC/MS, which, for routine quality controls in the perfume industry and in security areas, is undesirably slow and requires calibration. Alternative approaches, such as variants of ambient MS (e.g., electrospray ionization MS[59–61]), do not demand chemical derivatization or chromatographic separation, but require either liquid samples, a surface infused with the perfume (i.e., paper strip), or elaborate sample preparations. Overall, MS-based approaches typically require integration times of several seconds to minutes to achieve optimum sensitivities and the implementation of background subtraction procedures for quantitative results (i.e., non-absolute)[60,61]. Furthermore, the principal ingredients for (high-quality) perfumes are essential oils and organic synthetic aroma compounds. Essential oils, in particular, originate from natural sources, most typically plants, and, therefore, are generally chiral. They are also primary materials for the flavor,

health, and agriculture industries. Our approach, that includes no sample preparation and the ability for rapid trace chiral analysis, can be implemented for quality control (authentication, detecting adulteration) in all aforementioned commercial applications, including also the analysis of drugs, which largely consist of chiral compounds.

Third, we demonstrate online real-time chiral analysis of VOCs emitted by a biological organism under stress, in this case, a coniferous plant. The scientific challenge for modern atmospheric organic chemistry is to identify all available biogenic VOC (BVOC) sources and the physical and chemical processes determining the fate of volatile compounds, for a deeper understanding of their overall impact on atmosphere and climate[50]. To do so, accurate in-situ real-time measurements of the short- and long-term dynamics of BVOCs are necessary, and the chirality of the compounds has to become an integral aspect of the active research as their chirally specific dynamics (i.e., enantio-specific dynamics of different compounds, see **Fig.4C-D**), can serve as a unique signature for hitherto uncharacterized BVOC sources. Here we show how observations of chiral emissions from a coniferous plant following mechanical wounding can allow us to observe the enantiospecific dynamics of different compounds stored within the plant and even the resin that seals the wounding site. Such measurements are valuable in identifying— in situ and in real time — abiotic from biotic stress factors[34] and the underlying enzyme-driven response mechanisms[62]. Damage to boreal forests by bark-boring beetles generate chiral signals similar to those of mechanical stress (i.e., strong increase in (+) enantiomers) and recent observations in the Amazon forest of unusual enantiospecific changes of chiral BVOCs that have been attributed to insect proliferation[37]. Most crucially, real-time chiral analysis of VOCs emitted by plants can also enable the non-invasive health-status monitoring of plants and crops, contrary to the invasive electrophysiological measurements.

Numerous additional scientific and commercial applications can benefit from our approach, specifically concerning gas-phase chiral analysis. One prominent example is in the search of chirality — and potential chiral asymmetries — on celestial bodies (planets & comets) as a sign of life, where traditional chiral-sensing technologies such as chiral GC-MS (e.g., ESA's ROSETTA mission[63,64]), are currently employed. The inability to provide accurate, quantitative, results without calibration is vital for such searches and our approach can resolve these limitations. Finally, the concept of absolute chiral analysis can be extended to the nanoscale using recent developments in nanophotonic/plasmonic-based chirality sensitive schemes[65,66]. Such a possibility can enable the real-time in-situ investigation of chiral dynamics in the nanoscale such as the investigation of protein dynamics in situ. Most importantly, nanophotonic approaches open the possibility for ultraminiaturized systems of low-cost and low-energy-consumptions suitable for lab-on-a-chip devices.

Data availability

Data supporting the main findings of this work are available in the Supplementary Information files of this paper. The datasets generated and analyzed during the current study are available from the corresponding author on reasonable request.

Acknowledgements

This research was supported by the European Commission Horizon 2020, project ULTRACHIRAL (Grant No. FETOPEN-737071).

Author contributions

L.B. conceived the absolute chiral analysis concept and the experimental methodology, and together with J.W. conceived the experiments. L.B. designed the experiments, designed and constructed the CCP apparatus, performed all measurements and analyzed all results. J.B. conducted the sampling and analysis of VOCs using GC/MS. L.B. wrote the manuscript, and all authors discussed the results and contributed to the manuscript.

Competing interest declaration

L.B. and J. W. are inventors on a pending patent related to this work filed by the Johannes Gutenberg-Universität Mainz and the Max Planck Society. The other authors declare no competing financial interests.

Correspondence and requests for materials should be addressed to L.B.

Methods

Optical activity - Electromagnetic radiation propagating through a chiral medium experiences a complex index of refraction that differs in both its real and imaginary parts for right-circular (RCP) and left-circular polarization (LCP). Optical activity, i.e., the ability of a chiral medium to rotate and absorb linearly polarized light travelling through it, can be described by introducing a general form for the refractive index of the chiral medium that differs for RCP and LCP: $\varphi_c = \frac{\pi\, l}{\lambda}(n_L - n_R)$, with λ being the wavelength of light and l being the length of the chiral medium. The (complex) indices of refraction $n_{R/L}$ of the chiral medium for RCP and LCP, respectively, can be expressed as $n_{R/L} = n_c \mp \kappa$, with n_c the average (background) refractive index and κ the chirality ('Pasteur') parameter. The real part of κ [Re(κ)] is associated with effects of circular birefringence, while its imaginary part [Im(κ)] with effects of circular dichroism. The SOR values shown in **Fig.2A**, reflect the value of Re(κ), in the gas phase, for each presented compound. Our experimental approach allows for the precise measurement of both n_c and κ. Specifically for the chirality measurements presented here (Figs. 2-4), all results are proportional to Re(κ).

Experiment – The CCP device we use consists of a ring four-mirror optical cavity with the mirrors arranged in a bowtie configuration (**Fig.1**)[14–17]. Such an optical cavity supports two distinct counter-propagating laser beams, which we denote as clockwise (CW) and counter-clockwise (CCW) (according to their propagation within the cavity). The optical cavity has a total length of $L = 1.17$m and consists of highly reflective concave mirrors with radii of curvature of 1m (FiveNine Optics; specified reflectivity R~99.9% at 421 nm). A gas cell is positioned on one arm of the optical cavity and consists of a steel cylinder with a length of $l = 10$cm and an inner volume of 1.2mL. Two AR-coated SiO_2 windows (FiveNine Optics; AR coated with specified R < 0.01% per surface) are used to seal the gas cell. Under this configuration, the optical finesse of the cavity is: $\mathcal{F} \approx 400$. Gaseous mixtures (chiral vapours) are introduced into the gas cell via PEEK tubing. We use a 6.35mm thick, AR-coated, SiO_2 window as an intracavity magneto-optic crystal to generate Faraday-related circular birefringence, θ_F, with the use of permanent magnets attached directly to the mount holder of the substrate (in our case we obtain $\theta_F \approx 2°$)[67]. This intracavity Faraday rotation symmetrically splits the cavity resonances into two (orthogonal) circularly polarized cavity modes, i.e., one resonant for right circularly polarized light and the other for left circularly polarized light and, hence, denoted hereafter as R and L modes. The resulting R-L cavity modes are separated by $2f_F = 2\theta_F \cdot \frac{FSR}{\pi}$, where $FSR = \frac{c}{n\,L}$ is the cavity's free spectral range, c is the speed of light, L is the length of the cavity, and n the refractive index of the intracavity medium. In our experiments we obtain $f_F \approx 2.8$MHz. The intracavity Faraday circular birefringence also suppresses the effects of any possible intracavity linear birefringence[14–17], ensuring the conservation of the circular polarization character of the R-L modes. In the absence of any chiral substance, the R-L mode frequency splitting is identical for both CW and CCW propagation directions. The introduction of a chiral substance causes circular birefringence (φ_c), which causes the frequency splitting between the R and L modes to be different for the CW and CCW propagation directions, i.e., $\delta f_{CW} = 2|f_F + f_c|$ and $\delta f_{CCW} = 2|f_F - f_c|$, where $f_c = \varphi_c \cdot \frac{FSR}{\pi}$. Thus, the cavity-mode (frequency) spectrum consists of four distinct (non-degenerate) modes, R_{CW}, L_{CW}, R_{CCW}, L_{CCW}, which enables us to determine φ_c by directly measuring f_c. Measurement of the average refractive index, n_c, becomes possible through the direct measurement of the central frequencies of any of the cavity modes. To do so accurately, we servo-lock the emission frequency of the laser to a cavity resonance (in our experiments either R_{CW} or L_{CW}). In this case, the laser wavelength is fixed while its frequency tracks the changes in refractive index, since: $\delta f/f = -\delta n/n$[68,69]. From the gas refractivity measurements, we can then extract the density of the compound under investigation[27].

GC/CCP analysis – In all cases of GC/CCP analysis we use splitless injection (Agilent HP 6890A GC, Agilent Technologies, USA) of mixture solutions in ethanol (1μL of solution injected). The chiral separations of the monoterpene mixture (**Fig.2B**) and racemic limonene (**Fig. 2C**) were achieved using a 120 m β-DEX™ 120 column (Sigma-Aldrich GmbH, Germany) with 0.25 mm internal diameter and a 0.25 μm film thickness. The column flow was chosen to be 1.5ml/min and the temperature programme to be 40 °C for 4 minutes then 40 °C to 110 °C at 3.5 °C min^{-1}, 20min at 110 °C (isothermal), and 110 °C to 210 °C at 10 °C/min. For the OR-chromatogram of (R)-(-)-2-butanol (Fig.2D), we used a 60 m β-DEX™ 120 column (Sigma-Aldrich GmbH, Germany) with 0.25 mm internal diameter and a 0.25 μm film thickness. The column flow was chosen to be 2.5ml/min and the temperature programme to be 40 °C for 4 minutes then 40 °C to 100 °C at 5 °C min^{-1} and 100 °C to 210 °C at 30 °C/min. For the mixtures we use enantiopure (+)-α-pinene, (+)-α-pinene, (R)-(-)-α-phellandrene, (+)-limonene, (-)-limonene, (R)-(-)-2-butanol, and racemic camphene (all compounds purchased from Sigma Aldrich). For the measurements

shown in **Fig.2B** we prepare the following mixture: 120μL (+)-α-pinene, 100μL camphene, 20μL (R)-(-)-α-phellandrene, and 90μL (+)-limonene.

CCP-based chiral analysis of perfumes – All perfumes were purchased from local retail stores. The low-cost fragrance clones we use for quality comparison with the authentic ones are: '*Suddenly Madame Glamour*' by Lidl (***AC#1***), '*Magic*' by Miro (***AC#2***), and '*Madame Isabelle*' by La Rive (***AC#3***), as alternatives for '*Coco Mademoiselle*' by Chanel and '*Miss Dior*' by Dior; '*River of Love*' by La Rive (***AC#4***), '*Wish*' by Chopard (***AC#4***), and '*Diable Bleu*' by Creation Lamis (***AC#5***), as alternatives for '*Angel*' by Thierry Mugler; and '*Queen of Life*' (QoL) by La Rive (***AC#6***) as the alternative for '*La vie est belle*' (LVeB) by Lancôme. All perfume measurements are realized using dynamic air sampling with the help of a pump and a flow controller (Bronkhorst® F-201CV) that allows us to control and keep constant the sampling flow (sampling flow rates of ~30ml/min were used for the measurements). For the sampling and transfer lines we use PEEK tubing (inner diameter 0.74mm, Supelco Inc.).

CCP-based chiral analysis of chiral emissions from a plant – The *Pinus heldreichii* we use for our measurements was purchased from a local greenhouse (Blumenhaus Smedla, Mainz, Germany), and has a total height of ~80cm (**Fig. 4A**). We use a 25L Tedlar® sampling bag (ANALYT-MTC GmbH, Germany) secured around the tree stem to create an open-bottom sampling chamber that encloses the plant's upper branches (Fig. 4B; icons created with BioRender.com). This open-bottom design allows air to move between the interior and exterior of the enclosed space to avoid possible suffocation of the plant during sampling (we do not implement any active mixing of both air volumes), while we ensure that the sampling volume is located at a significant distance from the plant's soil (>10cm) to avoid signal contamination from the soil compartment. A heating tape supported around the sampling bag allows us to actively control the temperature within the sampling chamber (during the measurements we continuously monitor and keep stable the temperature within the sampling chamber, see **Fig. S5**). We ensure that the heating tape is not in contact with neither the branches nor the needles of the plant to avoid any contribution to the signal originating from possible local heat-induced damage. For the continuous online sampling we use a thermal desorption unit (TDU; TT24-7 x-r, Markes International), and we sample ~1L of ambient air from the chamber through the bag's valve. Using helium 6.0 as the carrier gas we transfer the desorbed sample through PEEK tubing (inner diameter 0.5mm, Supelco Inc.) to the intracavity gas cell for the CCP-based chirality measurements.

Offline chiral analysis using GC/MS – For the offline GC/MS analyses presented in this work we proceed as follows: for the perfume analysis, we fill scintillation vials (20mL) with ~0.2mL of perfume and use passive headspace sampling into sorbent tubes (typical exposure time ~15s). To sample the pine-plant emissions, we use a ¼ inch teflon sampling line placed inside the sampling bag, to which the sorbent tubes are connected to, outside the bag; samples are collected onto the sorbent cartridges at 200 ml min^{-1} for ~ 10 minutes using a GilAir Plus Personal Air Sampling Pump (Sensidyne®, USA). The sorbent cartridges, used in both cases, are made from inert coated stainless steel [SilcoNert 2000 (SilcoTek™, Germany)], and the sorbent consists of 150 mg of Tenax® TA followed by 150 mg of Carbograph™ 5 TD (560 m^2/g). The size of the Carbograph™ particles is in the range of 20-40 mesh. The Carbograph™ 5 was supplied by L.A.R.A s.r.l. (Rome, Italy) and the Tenax® by Buchem BV (Apeldoorn, The Netherlands). The cartridges are desorbed using a TD100-xr automated thermal desorption unit (Markes International Ltd, U.K.). The cartridges are first dry-purged with 50 ml/min of helium 6.0 carrier gas for 5 minutes to remove water before being desorbed with a flow 50 ml/min at 250 °C for 10 minutes. After cartridge desorption, the sample is transferred to the cold focusing trap (Material emissions cold trap, Markes International, U.K.) at 30 °C. The trap is purged with 50 ml min^{-1} of helium 6.0 carrier gas for 1 minute and is then desorbed at 250 °C for 3 minutes. Specifically for the measurements of the pine plant emissions, cartridges that are sampled before the pine tree branch was broken are desorbed with a split ratio of 221:1, whereas cartridges that are sampled after the branch breaking were desorbed with a split ratio of 1005:1. In all cases, the sample matrix was separated and detected using a GC/TOF-MS (GC 7890B, Agilent Technologies, U.S.A) (BenchToF-select, Markes Interntional Ltd, U.K.). The chiral separation is achieved using a 30 m β-DEX™ 120 column (Sigma-Aldrich GmbH, Germany) with 0.25 mm internal diameter and a 0.25 μm film thickness. The column flow is chosen to be 1 ml/min and the temperature programme to be 40 °C for 5 minutes then 40 °C to 150 °C at 4 °C min^{-1} until 220°C and then held again for 5 minutes. Identification of the target compounds was achieved by comparing the obtained mass spectra to the NIST database library and by spiking clean cartridges with the headspace from the relevant liquid standard. Each target compound was calibrated separately at each split ratio using a gas standard mixture (Apel-Riemer Environmental Inc., 2019) and liquid standards of chiral molecules.

References

1. Busch, K. W. & Busch, M. A. *Chiral Analysis*. (Elsevier Science, 2006).
2. Berova, N., Polavarapu, P. L., Nakanishi, K. & Woody, R. W. *Comprehensive chiroptical spectroscopy*. (John Wiley & Sons, 2012).
3. Polavarapu, P. L. *Chiral Analysis: Advances in Spectroscopy, Chromatography and Emerging Methods*. (Elsevier Science, 2018).
4. Janssen, M. H. M. & Powis, I. Detecting chirality in molecules by imaging photoelectron circular dichroism. *Phys. Chem. Chem. Phys.* **16,** 856–871 (2014).
5. Pitzer, M. *et al.* Direct Determination of Absolute Molecular Stereochemistry in Gas Phase by Coulomb Explosion Imaging. *Science (80-.).* **341,** 1096–1100 (2013).
6. Comby, A. *et al.* Real-time determination of enantiomeric and isomeric content using photoelectron elliptical dichroism. *Nat. Commun.* **9,** 5212 (2018).
7. Rhee, H. *et al.* Femtosecond characterization of vibrational optical activity of chiral molecules. *Nature* **458,** 310–313 (2009).
8. Patterson, D., Schnell, M. & Doyle, J. M. Enantiomer-specific detection of chiral molecules via microwave spectroscopy. *Nature* **497,** 475–477 (2013).
9. Tang, Y. & Cohen, A. E. Enhanced Enantioselectivity in Excitation of Chiral Molecules by Superchiral Light. *Science (80-.).* **332,** 333–336 (2011).
10. Hendry, E. *et al.* Ultrasensitive detection and characterization of biomolecules using superchiral fields. *Nat. Nanotechnol.* **5,** 783–787 (2010).
11. Manolis, A. The diagnostic potential of breath analysis. *Clin. Chem.* **29,** 5–15 (1983).
12. Boots, A. W. *et al.* The versatile use of exhaled volatile organic compounds in human health and disease. *J. Breath Res.* **6,** 27108 (2012).
13. Dudareva, N., Negre, F., Nagegowda, D. A. & Orlova, I. Plant Volatiles: Recent Advances and Future Perspectives. *CRC. Crit. Rev. Plant Sci.* **25,** 417–440 (2006).
14. Bougas, L., Katsoprinakis, G. E., von Klitzing, W., Sapirstein, J. & Rakitzis, T. P. Cavity-Enhanced Parity-Nonconserving Optical Rotation in Metastable Xe and Hg. *Phys. Rev. Lett.* **108,** 210801 (2012).
15. Bougas, L., Katsoprinakis, G. E., von Klitzing, W. & Rakitzis, T. P. Fundamentals of cavity-enhanced polarimetry for parity-nonconserving optical rotation measurements: Application to Xe, Hg, and I. *Phys. Rev. A* **89,** 52127 (2014).
16. Sofikitis, D. *et al.* Evanescent-wave and ambient chiral sensing by signal-reversing cavity ringdown polarimetry. *Nature* **514,** 76 (2014).
17. Bougas, L. *et al.* Chiral cavity ring down polarimetry: Chirality and magnetometry measurements using signal reversals. *J. Chem. Phys.* **143,** 104202 (2015).
18. Tran, D.-B.-A., Manfred, K. M., Peverall, R. & Ritchie, G. A. D. Continuous-Wave Cavity-Enhanced Polarimetry for Optical Rotation Measurement of Chiral Molecules. *Anal. Chem.* **93,** 5403–5411 (2021).
19. Spiliotis, A. K. *et al.* Gas-phase optical activity measurements using a compact cavity ringdown polarimeter. *Laser Phys.* **30,** 75602 (2020).
20. Hall, J. L., Ye, J. & Ma, L.-S. Measurement of mirror birefringence at the sub-ppm level: Proposed application to a test of QED. *Phys. Rev. A* **62,** 13815 (2000).
21. Bailly, G., Thon, R. & Robilliard, C. Highly sensitive frequency metrology for optical anisotropy measurements. *Rev. Sci. Instrum.* **81,** 33105 (2010).
22. Fleisher, A. J., Long, D. A., Liu, Q. & Hodges, J. T. Precision interferometric measurements of mirror birefringence in high-finesse optical resonators. *Phys. Rev. A* **93,** 13833 (2016).
23. Yu, X. & Yao, Z.-P. Chiral recognition and determination of enantiomeric excess by mass spectrometry: A review. *Anal. Chim. Acta* **968,** 1–20 (2017).
24. Müller, T., Wiberg, K. B., Vaccaro, P. H., Cheeseman, J. R. & Frisch, M. J. Cavity ring-down polarimetry (CRDP): theoretical and experimental characterization. *J. Opt. Soc. Am. B* **19,** 125–141 (2002).
25. Wilson, S. M., Wiberg, K. B., Cheeseman, J. R., Frisch, M. J. & Vaccaro, P. H. Nonresonant Optical Activity of Isolated Organic Molecules. *J. Phys. Chem. A* **109,** 11752–11764 (2005).
26. van Ruth, S. M. Methods for gas chromatography-olfactometry: a review. *Biomol. Eng.* **17,** 121–128 (2001).
27. Pendrill, L. R. Refractometry and gas density. *Metrologia* **41,** S40–S51 (2004).
28. Avalos, M. *et al.* Absolute Asymmetric Synthesis under Physical Fields: Facts and Fictions. *Chem. Rev.* **98,** 2391–2404 (1998).
29. Shukla, N. & Gellman, A. J. Chiral metal surfaces for enantioselective processes. *Nat. Mater.* **19,** 939–945 (2020).
30. Tassinari, F. *et al.* Enantioseparation by crystallization using magnetic substrates. *Chem. Sci.* **10,** 5246–5250

(2019).
31. Do, T. K. T., Hadji-Minaglou, F., Antoniotti, S. & Fernandez, X. Authenticity of essential oils. *TrAC Trends Anal. Chem.* **66,** 146–157 (2015).
32. Sindelarova, K. *et al.* Global data set of biogenic VOC emissions calculated by the MEGAN model over the last 30 years. *Atmos. Chem. Phys.* **14,** 9317–9341 (2014).
33. Zhang, H. *et al.* Monoterpenes are the largest source of summertime organic aerosol in the southeastern United States. *Proc. Natl. Acad. Sci.* **115,** 2038–2043 (2018).
34. Holopainen, J. K. & Gershenzon, J. Multiple stress factors and the emission of plant VOCs. *Trends Plant Sci.* **15,** 176–184 (2010).
35. Loreto, F., Dicke, M., Schnitzler, J.-P. & Turlings, T. E. D. C. J. Plant volatiles and the environment. *Plant. Cell Environ.* **37,** 1905–1908 (2014).
36. Williams, J. Organic Trace Gases in the Atmosphere: An Overview. *Environ. Chem.* **1,** 125–136 (2004).
37. Zannoni, N. *et al.* Surprising chiral composition changes over the Amazon rainforest with height, time and season. *Commun. Earth Environ.* **1,** 4 (2020).
38. Renwick, J. A., Hughes, P. R. & Krull, I. S. Selective production of cis- and trans-verbenol from (-)-and (+)-alpha by a bark beetle. *Science (80-.).* **191,** 199–201 (1976).
39. Norin, T. Chiral chemodiversity and its role for biological activity. Some observations from studies on insect/insect and insect/plant relationships. *Pure Appl. Chem.* **68,** 2043–2049 (1996).
40. He, J. *et al.* An unbiased approach elucidates variation in (S)-(+)-linalool, a context-specific mediator of a tri-trophic interaction in wild tobacco. *Proc. Natl. Acad. Sci.* **116,** 14651–14660 (2019).
41. Runyon, J. B., Mescher, M. C. & De Moraes, C. M. Volatile Chemical Cues Guide Host Location and Host Selection by Parasitic Plants. *Science (80-.).* **313,** 1964–1967 (2006).
42. Baldwin, I. T., Halitschke, R., Paschold, A., von Dahl, C. C. & Preston, C. A. Volatile Signaling in Plant-Plant Interactions: 'Talking Trees' in the Genomics Era. *Science (80-.).* **311,** 812–815 (2006).
43. Heil, M. & Karban, R. Explaining evolution of plant communication by airborne signals. *Trends Ecol. Evol.* **25,** 137–144 (2010).
44. Williams, J., Yassaa, N., Bartenbach, S. & Lelieveld, J. Mirror image hydrocarbons from Tropical and Boreal forests. *Atmos. Chem. Phys.* **7,** 973–980 (2007).
45. Song, W. *et al.* Winter and summer characterization of biogenic enantiomeric monoterpenes and anthropogenic BTEX compounds at a Mediterranean Stone Pine forest site. *J. Atmos. Chem.* **68,** 233–250 (2011).
46. Yassaa, N. *et al.* Diel cycles of isoprenoids in the emissions of Norway spruce, four Scots pine chemotypes, and in Boreal forest ambient air during HUMPPA-COPEC-2010. *Atmos. Chem. Phys. Discuss.* **12,** 10425–10460 (2012).
47. Pureswaran, D. S., Gries, R. & Borden, J. H. Quantitative variation in monoterpenes in four species of conifers. *Biochem. Syst. Ecol.* **32,** 1109–1136 (2004).
48. Sjödin, K., Persson, M., Fäldt, J., Ekberg, I. & Borg-Karlson, A.-K. Occurrence and Correlations of Monoterpene Hydrocarbon Enantiomers in Pinus sylvestris and Picea abies. *J. Chem. Ecol.* **26,** 1701–1720 (2000).
49. Staudt, M., Byron, J., Piquemal, K. & Williams, J. Compartment specific chiral pinene emissions identified in a Maritime pine forest. *Sci. Total Environ.* **654,** 1158–1166 (2019).
50. Glasius, M. & Goldstein, A. H. Recent Discoveries and Future Challenges in Atmospheric Organic Chemistry. *Environ. Sci. Technol.* **50,** 2754–2764 (2016).
51. Fäldt, J., Solheim, H., Långström, B. & Borg-Karlson, A.-K. Influence of Fungal Infection and Wounding on Contents and Enantiomeric Compositions of Monoterpenes in Phloem of Pinus sylvestris. *J. Chem. Ecol.* **32,** 1779 (2006).
52. Woolfenden, E. Monitoring VOCs in Air Using Sorbent Tubes Followed by Thermal Desorption-Capillary GC Analysis: Summary of Data and Practical Guidelines. *J. Air Waste Manage. Assoc.* **47,** 20–36 (1997).
53. Sheu, R. *et al.* Advances in offline approaches for chemically speciated measurements of trace gas-phase organic compounds via adsorbent tubes in an integrated sampling-to-analysis system. *J. Chromatogr. A* **1575,** 80–90 (2018).
54. Eerdekens, G. *et al.* VOC measurements within a boreal forest during spring 2005: on the occurrence of elevated monoterpene concentrations during night time intense particle concentration events. *Atmos. Chem. Phys.* **9,** 8331–8350 (2009).
55. Yassaa, N. & Williams, J. Analysis of enantiomeric and non-enantiomeric monoterpenes in plant emissions using portable dynamic air sampling/solid-phase microextraction (PDAS-SPME) and chiral gas chromatography/mass spectrometry. *Atmos. Environ.* **39,** 4875–4884 (2005).

56. Grote, R. & Niinemets, Ü. Modeling Volatile Isoprenoid Emissions – A Story with Split Ends. *Plant Biol* **9,** e42–e59 (2007).
57. Ghirardo, A. *et al.* Determination of de novo and pool emissions of terpenes from four common boreal/alpine trees by 13CO2 labelling and PTR-MS analysis. *Plant. Cell Environ.* **33,** 781–792 (2010).
58. Niinemets, Ü. *et al.* Estimations of isoprenoid emission capacity from enclosure studies: measurements, data processing, quality and standardized measurement protocols. *Biogeosciences* **8,** 2209–2246 (2011).
59. Cooks, R. G., Ouyang, Z., Takats, Z. & Wiseman, J. M. Ambient Mass Spectrometry. *Science (80-.).* **311,** 1566 LP-1570 (2006).
60. Marques, L. de A., Catharino, R. R., Bruns, R. E. & Eberlin, M. N. Electrospray ionization mass spectrometry fingerprinting of perfumes: rapid classification and counterfeit detection. *Rapid Commun. Mass Spectrom.* **20,** 3654–3658 (2006).
61. Chingin, K., Gamez, G., Chen, H., Zhu, L. & Zenobi, R. Rapid classification of perfumes by extractive electrospray ionization mass spectrometry (EESI-MS). *Rapid Commun. Mass Spectrom.* **22,** 2009–2014 (2008).
62. Savatin, D. V, Gramegna, G., Modesti, V. & Cervone, F. Wounding in the plant tissue: the defense of a dangerous passage . *Frontiers in Plant Science* **5,** 470 (2014).
63. Thiemann, W. H.-P. & Meierhenrich, U. ESA Mission ROSETTA Will Probe for Chirality of Cometary Amino Acids. *Orig. life Evol. Biosph.* **31,** 199–210 (2001).
64. Meierhenrich, U. J. *et al.* Evaluating the robustness of the enantioselective stationary phases on the Rosetta mission against space vacuum vaporization. *Adv. Sp. Res.* **52,** 2080–2084 (2013).
65. Droulias, S. & Bougas, L. Surface Plasmon Platform for Angle-Resolved Chiral Sensing. *ACS Photonics* **6,** 1485–1492 (2019).
66. Droulias, S. & Bougas, L. Absolute Chiral Sensing in Dielectric Metasurfaces Using Signal Reversals. *Nano Lett.* **20,** 5960–5966 (2020).
67. Visschers, J. C., Tretiak, O., Budker, D. & Bougas, L. Continuous-wave cavity ring-down polarimetry. *J. Chem. Phys.* **152,** 164202 (2020).
68. Eickhoff, M. L. & Hall, J. L. Real-time precision refractometry: new approaches. *Appl. Opt.* **36,** 1223–1234 (1997).
69. Egan, P. & Stone, J. A. Absolute refractometry of dry gas to ±3 parts in 10^9. *Appl. Opt.* **50,** 3076–3086 (2011).
70. Durand, M., Morville, J. & Romanini, D. Shot-noise-limited measurement of sub-parts-per-trillion birefringence phase shift in a high-finesse cavity. *Phys. Rev. A* **82,** 31803 (2010).
71. Dupré, P. Birefringence-induced frequency beating in high-finesse cavities by continuous-wave cavity ring-down spectroscopy. *Phys. Rev. A* **92,** 53817 (2015).

Supplementary Information for:
Absolute chiral analysis via cavity-enhanced polarimetry

Lykourgos Bougas[1*], Joseph Byron[2], Dmitry Budker[1,3,4], and Jonathan Williams[2,5]

[1] *Institut für Physik, Johannes Gutenberg-Universität Mainz, Mainz, Germany*
[2] *Max Planck Institute for Chemistry, Atmospheric Chemistry Department, Mainz, Germany*
[3] *Helmholtz Institute Mainz, GSI Helmholtzzentrum für Schwerionenforschung, Darmstadt, Germany*
[4] *Department of Physics, University of California, Berkeley, CA, USA*
[5] *Climate and Atmosphere Research Center, The Cyprus Institute, Nicosia, Cyprus.*
**** Correspondence should be addressed to: bougas.lykourgos@gmail.com***

I. Specific optical rotation of chiral compounds

In Table 1 we provide the values for the specific optical rotation (SOR) $[\alpha]_{421nm}^{21^o}$ of all the different chiral compounds we present and are relevant to our work.

Table 1 | Chemical properties of chiral volatile organic compounds.

	Formula	Molar mass [gr/mol]	Boiling point [°C]	Vapour pressure @ 21 °C [mbar]	$[\alpha]_{421nm}^{21^o}$ [deg. (gr/ml)$^{-1}$ dm^{-1}]
(R)-(-)-2-butanol	$C_4H_{10}O$	74.12	100	12.0	-(23.0± 0.8)
(+)-α-pinene	$C_{10}H_{16}$	136.24	156	4	123.2 ± 1.3
(+)-camphene			159	3	53.9 ± 1.2
(-)-β-pinene			166	3	16.2 ± 2.2
(R)-(-)-α-phellandrene			172	1	-(686.8 ± 1.1)
(R)-(+)-limonene			177	0.8-1.3	184.6 ± 1.8

II. Supplementary Data

A. GC/CCP analysis of enantiopure (±)-limonene

In **Fig. S1** we present GC/CCP-based analysis of enantiopure (+)- and (-)-limonene. For our analysis we use splitless injection (Agilent HP 6890A GC, Agilent Technologies, USA) of mixture solutions in ethanol (1μL of solution injected). The chiral separations were achieved using a 30m β-DEX™ 120 column (Sigma-Aldrich GmbH, Germany) with 0.25 mm internal diameter and a 0.25 μm film thickness. The column flow was chosen to be 8ml/min and the temperature programme to be 40 °C for 2 minutes then 40 °C to 210 °C at 12 °C min^{-1}. We use these results, under the 'GC' label, in our comparison with direct total sample measurements of enantiopure limonene in **Fig.2C** of the main text.

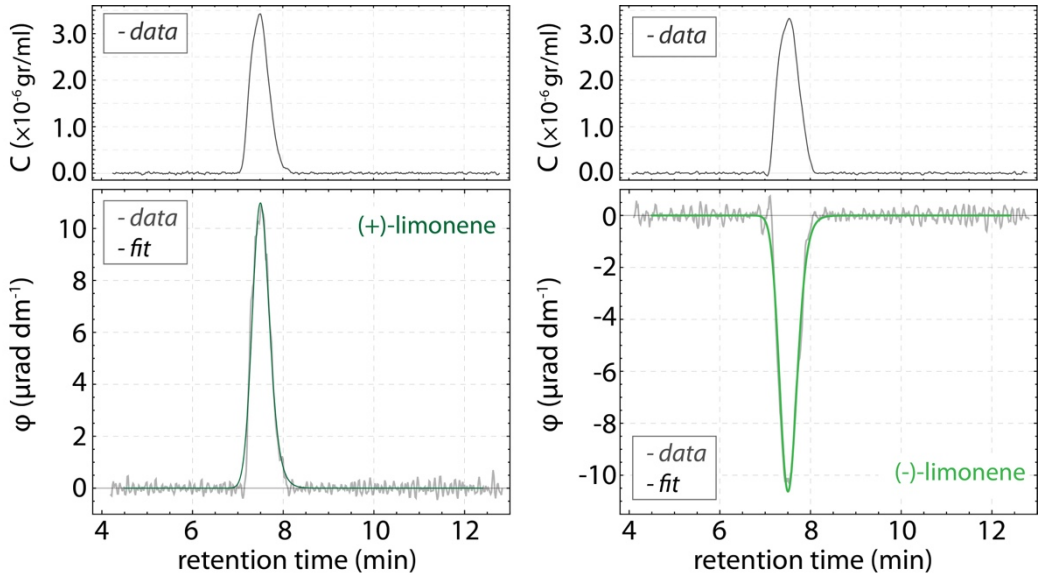

Figure S1 | GC/CCP-based chiral analysis of enantiopure (+)-limonene (*left*) and (-)-limonene (*right*). The analysis is performed under identical conditions as for the case of racemic limonene shown in Fig.2C of the main text.

B. Offline chiral analysis of perfumes using GC-MS

We select the commercially available low-cost fragrance clones according to advertised information provided by their respective production companies, in connection to publicly available information concerning fragrance clones.[3]

In the following figures we present the GC/MS analysis of all the perfumes used in this work, both the authentic and the low-cost fragrance clones. We use an identical separation method for all perfumes, designed specifically for the optimal separation of chiral monoterpenes and monoterpenoids. The chiral

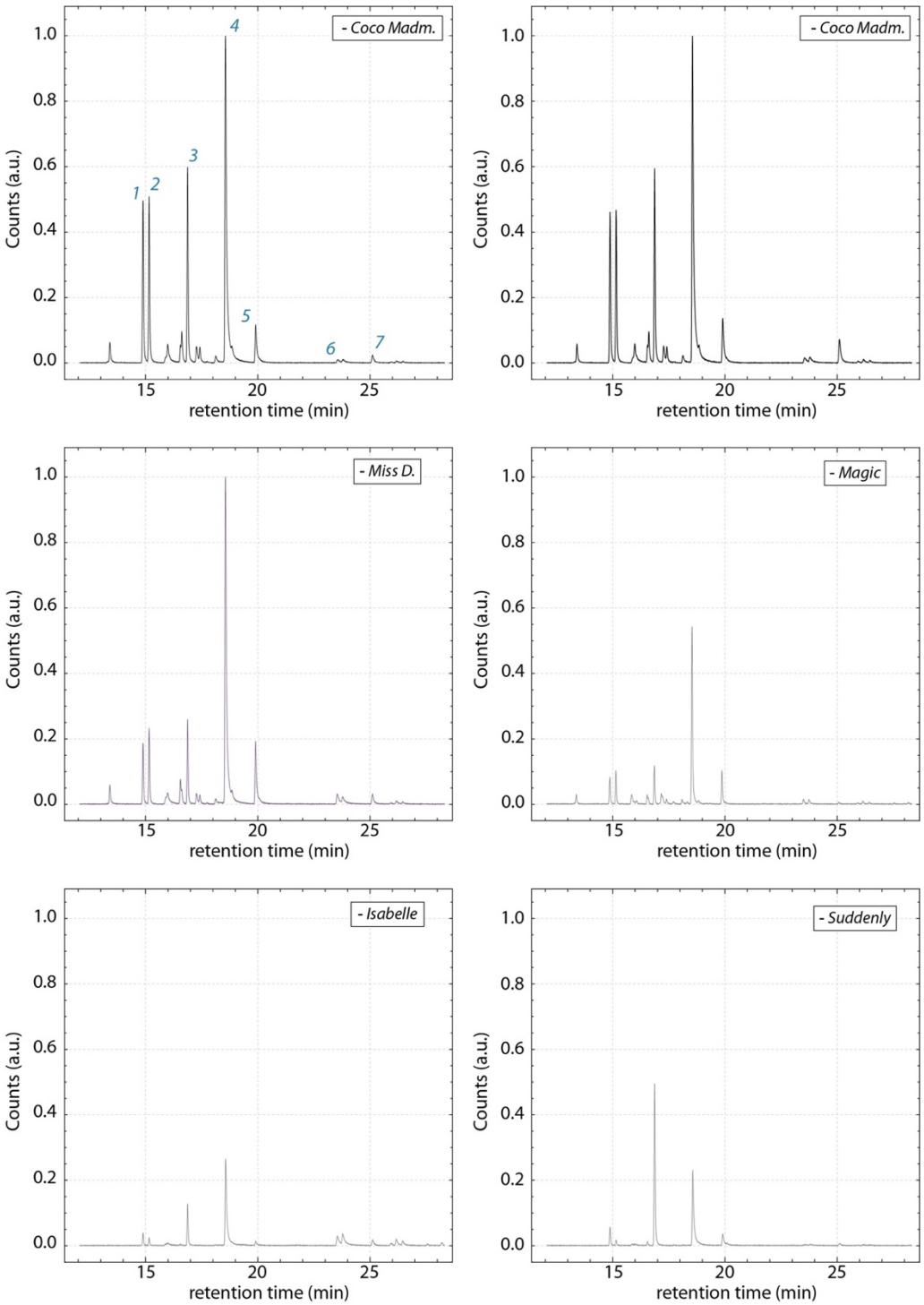

Figure S2 | Chromatograms for the perfumes: '*Coco Mademoiselle*' by Chanel (EdP) ('CM' in the main text); '*Miss Dior*' by Dior (EdP) ('MD'); '*Magic*' by Miro ('AC#1'); '*Madame Isabelle*' by La Rive ('AC#2'); and '*Suddenly Madame Glamour*' by Lidl ('AC#3'). Samples are collected from the headspace of 20ml scintillation vials that contain ~1mL of perfume. For ease of comparison, we normalize the signals of each spectra to the maximum signal value of (+)-limonene (peak 4) of the first spectrum of '*Coco Mademoiselle*'.

[3] www.duftzwillinge.eu; www.parfumo.net/Parfums/Dupes; duft-check.de.

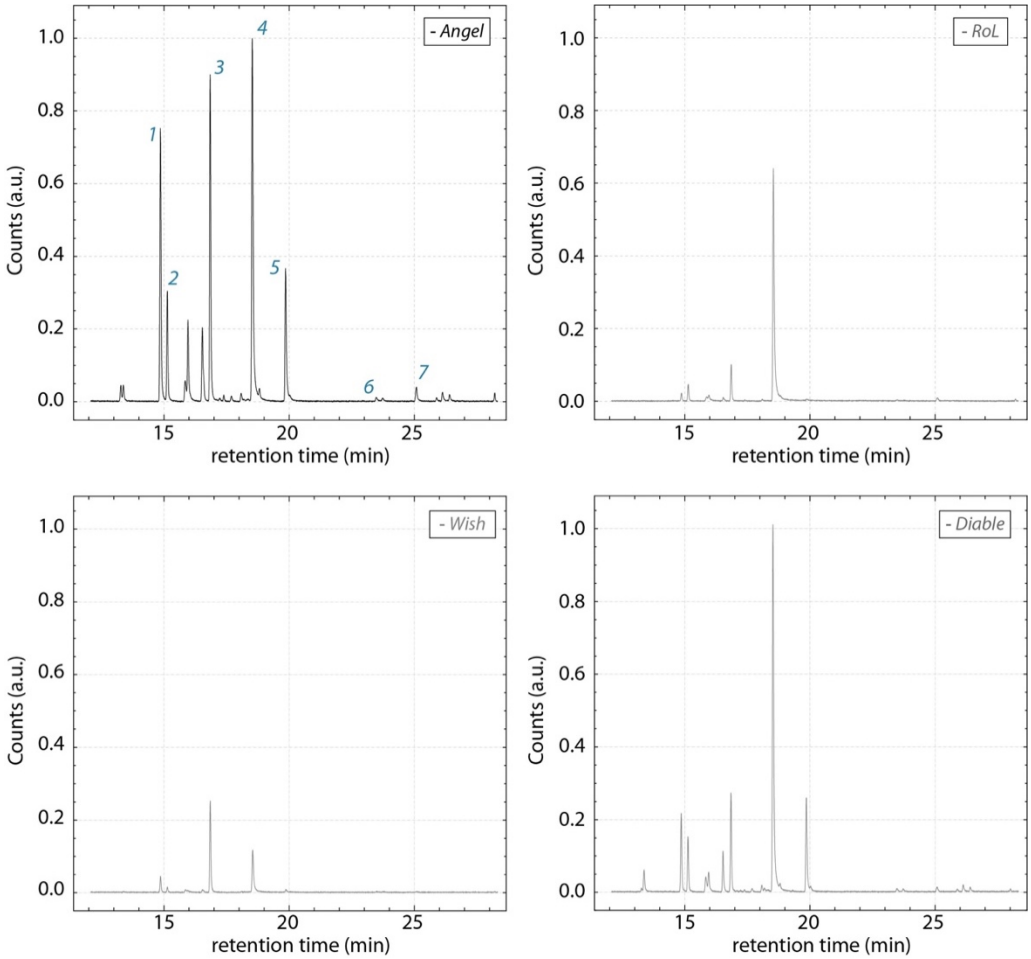

Figure S3 | Chromatograms of the perfumes: '*Angel*' by Thiery Mugler (EdP) ('Ang'); '*River of Love*' (RoL) by La Rive (EdP) ('AC#3' in the main text); '*Wish*' by Chopard (EdP) ('AC#4'); and '*Diable Bleu*' by Creation Lamis (EdP) ('AC#5'). Samples are collected from the headspace of 20ml scintillation vials that contain ~1mL of perfume, by sampling into homemade cartridges. For ease of comparison, we normalize the signals of each spectra to the maximum signal value of (+)-limonene (peak 4) of the first spectrum of '*Angel*'.

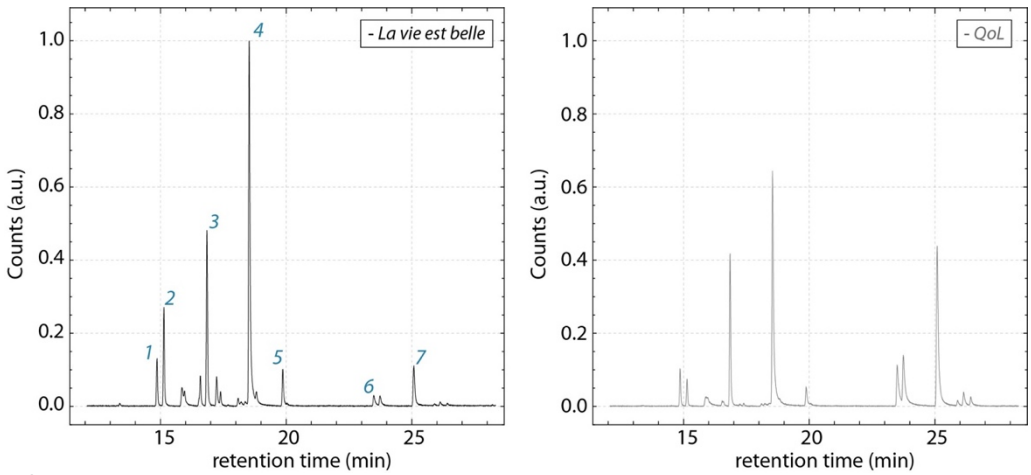

Figure S4 | Chromatograms of the perfumes: '*La vie est belle*' by Lancôme (EdP) ('LVeB'), and '*Queen of Life*' (QoL) by La Rive (EdP) ('AC#6'). Samples are collected from the headspace of 20ml scintillation vials that contain ~1mL of perfume, by sampling into homemade cartridges. For ease of comparison, we normalize the signals of each spectra to the maximum signal value of (+)-limonene (peak 4) of the spectrum of '*La vie est belle*'.

separations were achieved using a 30m β-DEX™ 120 column (Sigma-Aldrich GmbH, Germany) with 0.25 mm internal diameter and a 0.25 µm film thickness. The column flow was chosen to be 1ml/min and the temperature programme consists of an initial 5min step where the oven temperature is held at 40 °C, after which it was increased at a rate of 4 °C/min from 40 °C to 220 °C and then held again for 5 minutes.

In **Figs.S2-S4**, the presented labelled peaks correspond to: ***1*** (-)-α-pinene; ***2*** (+)-α-pinene; ***3*** (-)-β-pinene; ***4*** (+)-limonene; ***5*** (-)-limonene; ***6*** (-)-linalool followed by (+)-linalool (retention times of 23.54 min and 23.79 min, respectively, for the chromatogram of 'CM' shown in **Fig. S2**); and ***7*** linalyl acetate (achiral).

C. Chiral analysis of volatile emissions of a coniferous plant

1. Temperature and humidity measurements

We use a 25L Tedlar® sampling bag (ANALYT-MTC GmbH, Germany) secured around the tree stem to create an open-bottom sampling chamber that encloses the plant's upper branches. This open-bottom design allows air to move between the interior and exterior of the enclosed space to avoid possible suffocation of the plant during sampling (we do not implement any active mixing of both air volumes). A heating tape supported around the sampling bag allows us to actively control the temperature within the sampling chamber. We use a temperature and humidity logger device (TSP01, Thorlabs GmbH) to record the relative humidity in the laboratory and the temperature inside and outside the sampling chamber. We present our recordings for the whole duration of our measurements in Fig.S6, showing an overall stability of the laboratory humidity and the temperature inside the chamber during the measurements.

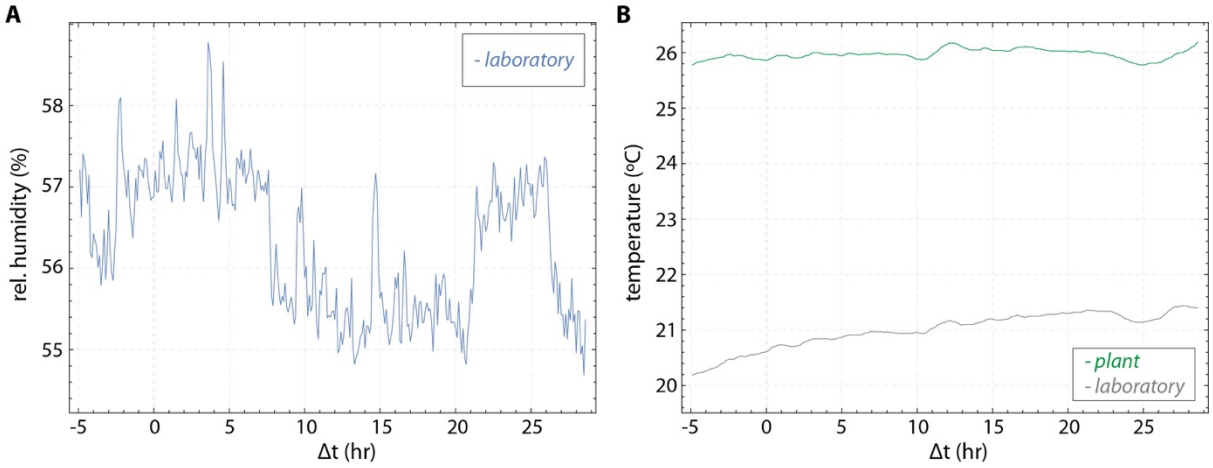

Figure S5 | Relative humidity measurements (%) of the laboratory's environment (**A**), and temperature measurements within and outside (i.e., laboratory temperature) the chamber that encloses the branches of the plant (**B**).

2. Estimation of overall concentration changes and effective specific optical rotation signal from GC/MS analysis

To sample the plant emissions, we use a ¼ inch teflon sampling line placed inside the sampling chamber (**Fig.4** main text). Samples are collected onto sorbent cartridges at 200 ml min^{-1} using a GilAir Plus Personal Air Sampling Pump (Sensidyne®, USA). We collect four samples before the mechanical wounding, i.e., branch cut, with a sampling time of ~10min. Following wounding, we collect two or three consecutive samples approximately every hour for 11 hrs, and two additional samples after 24hrs (sampling time ~10min). For the resin data, we collect two samples directly from the exposed wounding site (sampling time ~5min). In **Fig.S6** we reproduce the chromatogram of a sample collected before wounding (as shown also in **Fig.4** of the main text).

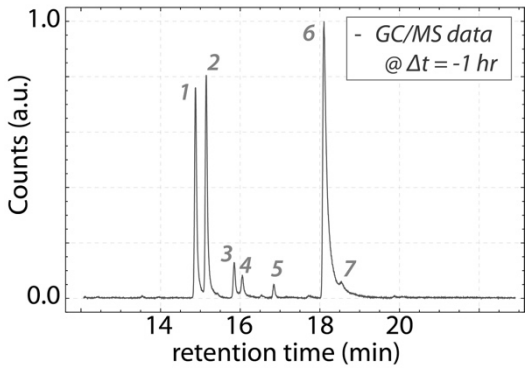

Figure S6 | Chromatogram of sample collected before wounding. The labeled monoterpene compounds correspond to: **1** (-)-α-pinene; **2** (+)-α-pinene; **3** (-)-camphene; **4** (+)-camphene; **5** (-)-β-pinene; **6** (-)-limonene; **7** (+)-limonene.

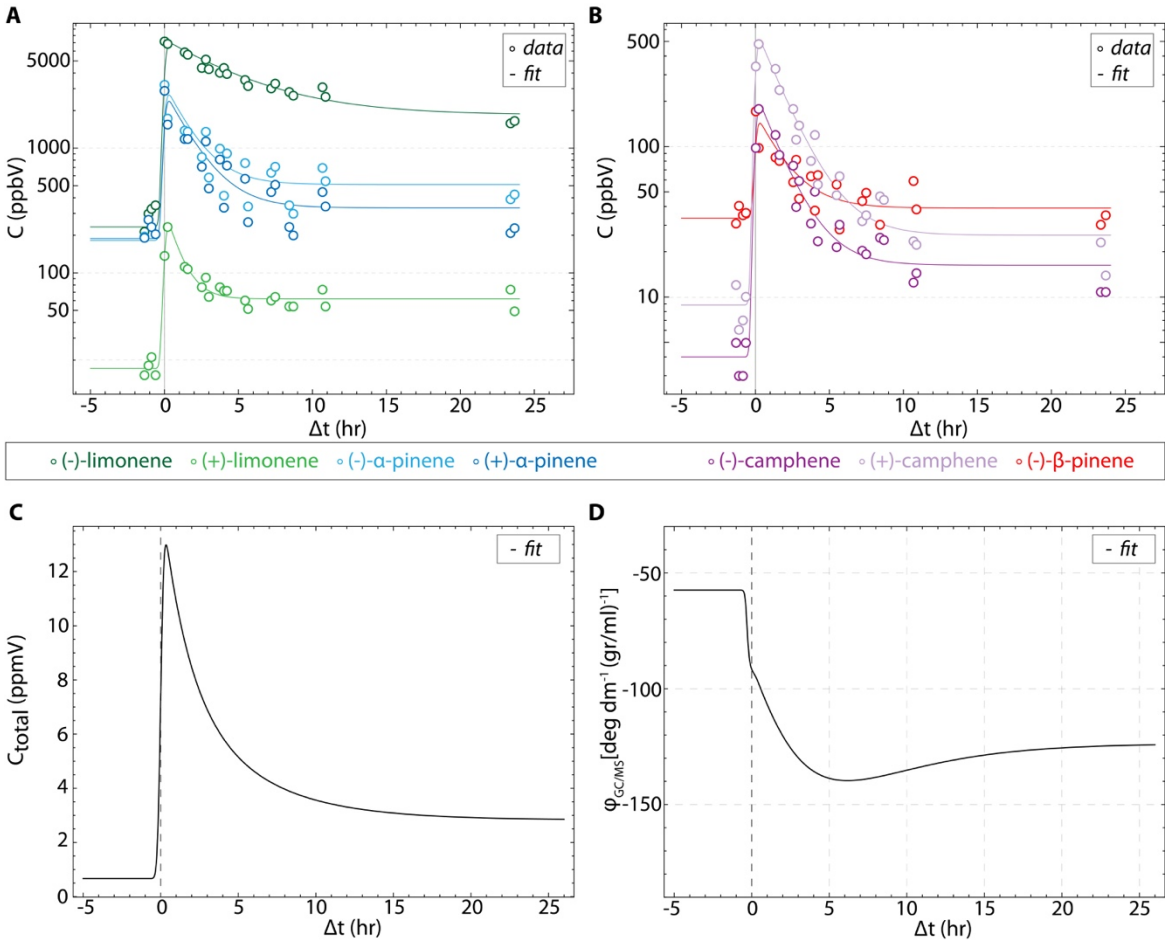

Figure S7 | Time dependent behavior of the concentration of the dominant monoterpene VOCs in the plant emissions, pre- and post-wounding, obtained through an offline GC/MS analysis: (±)-α-pinene and (±)-limonene (**A**), and (±)-camphene and (-)-β-pinene (**B**). **C**. Time dependent behavior of the overall concentration of the emissions as estimated from the measurements in **A** and **B**. **D.** Normalized chiroptical signal (effective specific optical rotation) as predicted from the individual GC/MS concentration measurements.

We analyze the samples using the offline GC/MS analysis procedure described in the main text. We use a non-linear, least-square minimization method to fit the observed time-dependent behavior of the concentration of each of the dominant monoterpene VOCs observed (pre- and post-wounding), as this extracted from the GC/MS analysis, using the following model function:

$$C_i(t) = \frac{A}{2} \times \left(exp\left[\frac{1}{2} \cdot \left(\frac{\sigma}{\tau} \right)^2 - \frac{t - t_0}{\tau} \right] + c \right) \times erfc\left[\frac{1}{\sqrt{2}} \left(\frac{\sigma}{\tau} - \frac{t - t_0}{\sigma} \right) \right],$$

where C_i is the concentration of the *i*th chiral VOC ($i = \{1,7\}$) and t is the time (independent) variable. This model results from the convolution of a mono-exponential decaying function (characteristic decay constant τ) starting at $t = t_0$, $H(t - t_0) \times A\ exp(-\frac{t-t_0}{\tau})$ [$H(t - t_0)$ is the Heaviside step function], with a normalized Gaussian function of standard deviation σ, which accounts for the sampling time. In addition, $erfc$ is the complementary error function, A a proportionality constant and c an offset parameter accounting for the observed plateau.

Using the specific optical rotation $[\alpha]^{21^o}_{421nm}$value (Table I) for each of the dominant chiral monoterpenes observed in the plant emissions, we can then calculate an *effective* expected specific optical rotation signal from the GC/MS analysis as follows:

$$\varphi_{GC/MS}(t)\ [deg\ (gr/ml)^{-1} dm^{-1}] = \frac{1}{\sum_i C_i(t)} \sum_i [a]_i \cdot l \cdot C_i(t)\ .$$

In **Fig.4C** and **Fig.4D** of the main text we present the results for $C_{total}(t) = \sum_i C_i(t)$ and $\varphi_{GC/MS}(t)$, respectively, that are in agreement with our CCP-based online chiroptical measurements. We reproduce these results in **Fig.S7** for clarity.

3. Photo of the damaged plant branch

In **Fig.S8** we present a photo of the damaged branch of the *Pinus heldreichii* we used for the measurements (shown also in **Fig.4** of the main text). The resin covering the wounding site can be clearly seen in the photo. Samples of the emissions of the resin (**Fig.4C,D** of the main text) are taken directly from the exposed wounding site.

Figure S8 | Photo of the damaged branch of the plant used in our measurements, i.e., *Pinus heldreichii*. The resin that hardens to seal the wound site is clearly visible.